Environmental Science & Technology

Article

Cite This: Environ. Sci. Technol. 2019, 53, 10258−10268

pubs.acs.org/est

Simulating and Quantifying Multiple Natural Subsea CO_2 Seeps at Panarea Island (Aeolian Islands, Italy) as a Proxy for Potential Leakage from Subseabed Carbon Storage Sites

Jonas Gros,*[,†] Mark Schmidt,[†] Andrew W. Dale,[†] Peter Linke,[†] Lisa Vielstädte,[†] Nikolaus Bigalke,[†,‡] Matthias Haeckel,[†] Klaus Wallmann,[†] and Stefan Sommer[†]

[†]GEOMAR Helmholtz Centre for Ocean Research Kiel, RD2/Marine Geosystems Wischhofstrasse 1-3, D-24148 Kiel, Germany

Supporting Information

ABSTRACT: Carbon dioxide (CO_2) capture and storage (CCS) has been discussed as a potentially significant mitigation option for the ongoing climate warming. Natural CO_2 release sites serve as natural laboratories to study subsea CO_2 leakage in order to identify suitable analytical methods and numerical models to develop best-practice procedures for the monitoring of subseabed storage sites. We present a new model of bubble (plume) dynamics, advection-dispersion of dissolved CO_2, and carbonate chemistry. The focus is on a medium-sized CO_2 release from 294 identified small point sources around Panarea Island (South-East Tyrrhenian Sea, Aeolian Islands, Italy) in water depths of about 40−50 m. This study evaluates how multiple CO_2 seep sites generate a temporally variable plume of dissolved CO_2. The model also allows the overall flow rate of CO_2 to be estimated based on field measurements of pH. Simulations indicate a release of ∼6900 t y^{-1} of CO_2 for the investigated area and highlight an important role of seeps located at >20 m water depth in the carbon budget of the Panarea offshore gas release system. This new transport-reaction model provides a framework for understanding potential future leaks from CO_2 storage sites.

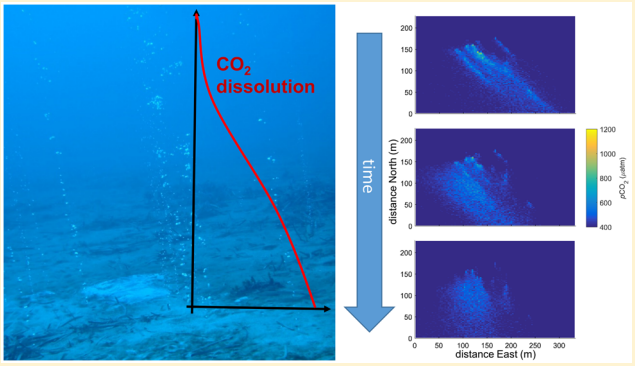

INTRODUCTION

Carbon dioxide (CO_2) capture and storage (CCS) has been discussed as a potentially key tool in the stringent mitigation required to restrict climate warming to within 2 °C relative to preindustrial levels.[1,2] CCS represents the capture of CO_2 mainly from large point sources and its injection into subsurface reservoirs, usually at 800−2000 m below the seafloor.[1,3−5] In Europe, CO_2 storage capacity is chiefly located offshore within sandstone aquifers.[6,7] Currently, this storage capacity lies principally within Norwegian waters, where the multinational energy company Equinor (formerly Statoil ASA) operates the *Sleipner* CCS facility that has injected ∼1 Mt y^{-1} of CO_2 into the Utsira formation since 1996.[8,9] Procedures guide the selection of appropriate subseabed CO_2 storage sites,[5,10−12] which have been suggested to present lower risks for human populations in case of accidental leakage compared to terrestrial locations.[13,14] However, there is a need to identify suitable procedures for the monitoring of active and closed marine storage sites to ensure their adequate operation and enable identification and quantification of potential leaks.[15]

Diverse potential scenarios of subsea CO_2 leaks have been simulated.[16−20] This includes large CO_2 releases resulting from a massive failure of a facility (e.g., a blowout).[19] The high daily release of 10,000 t d^{-1} of CO_2 from a point source in the North Sea for a full year was predicted to reduce pH by 0.25 units up to 141 km away from the source, and by >2 units nearer to the source. The magnitude of such releases makes it unlikely that they could remain undetected or ignored for prolonged periods. On the contrary, smaller gas leaks remain largely ignored, such as the release of 5−70 t d^{-1} of methane at the 22/4b blowout crater in the UK North Sea, more than 20 years after the 1990 accidental blowout,[21,22] or the widespread natural gas seepage resulting from offshore oil and gas activities.[23,24]

In the absence of strong bubble plumes, the high solubility of CO_2 leads to its rapid aqueous dissolution from bubbles within a few meters of their emission into the sea as indicated by field and laboratory data, and model simulations.[13,16,20,25−27] Consequently, small CO_2 leaks disperse in ambient seawater over short distances[20,28] and are therefore particularly challenging to detect without careful monitoring techniques.[20] For example, a recent study indicated that the detectability of a relatively low leakage rate of gaseous CO_2 of

Received: April 9, 2019
Revised: July 24, 2019
Accepted: July 25, 2019
Published: August 21, 2019

DOI: 10.1021/acs.est.9b02131
Environ. Sci. Technol. 2019, 53, 10258−10268

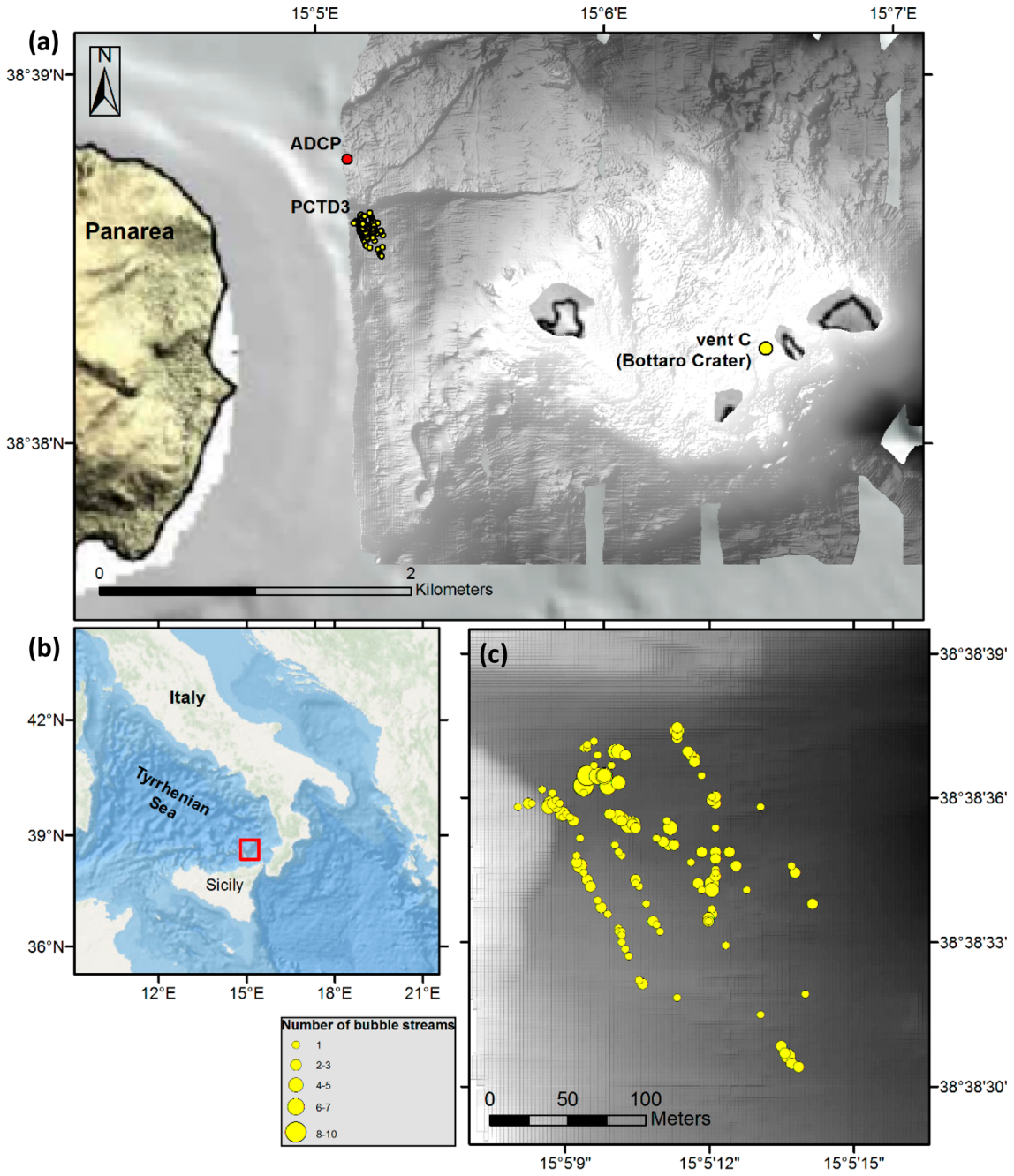

Figure 1. (a) Position of the two study sites (station PCTD3 and Bottaro crater) offshore Panarea, and (b) position of Panarea Island offshore Italy in the South-East Tyrrhenian Sea. The position of the ADCP instrument is also indicated. (c) A zoom on station PCTD3 indicates the 130 venting sites identified by video recording. The diameter of the circles is proportional to the number of identified bubble streams per site (up to 10 per site, 294 in total). High-resolution bathymetry offshore Panarea[112] was plotted with ArcGIS 10.2.

85 kg d^{-1} would be limited to < 30 m horizontal distance from the release source and ≤ 2 m from the seafloor.[20] Nevertheless, such small single-source releases of CO_2 were evaluated as largely insignificant in terms of storage performance, and a single leak of this magnitude would therefore not prevent CCS sites from retaining a millennium climate mitigation effect.[20] However, migration pathways within geological formations and overlying sediments may lead to numerous, spatially distributed emission sources under some circumstances.[14,29] There is concern that several small-sized leaks may remain undetected under these conditions. Being able to ensure leak detection and flow rate determination is particularly important for monitoring of storage sites because major leaks may offset the benefits of energy-intensive CCS facilities.[1,30−32]

At present, two alternative, complementary strategies exist to investigate the impact of potential subsea CO_2 leaks: experimental releases and natural CO_2 seeps. Manmade subsea (bed) experimental releases of CO_2 require costly logistics and afford limited distribution of emission source(s).[15,20,33,34] Natural CO_2 seepages[13,17,29,35−38] exhibit less-constrained flow rates and may present more spatially distributed emission sources. The seep system offshore Panarea Island (Aeolian Islands, South Italy) is one of the most easily accessible natural

DOI: 10.1021/acs.est.9b02131
Environ. Sci. Technol. 2019, 53, 10258−10268

seeps[25,29,36,39−42] and was selected for this study as a realistic leakage analogue.

Here, we use field data collected in May 2014 at a natural CO_2 seep site covering ∼18,000 m^2 offshore Panarea during cruise POS469 of the R/V *Poseidon*[29,43] to provide insights about the possible geochemical impacts of CO_2 leaks from subseabed storage reservoirs. A new simulation tool is developed and validated with field data. This model builds on the existing multiphase bubble and droplet plume model Texas A&M oil spill (outfall) calculator (TAMOC).[44−50] Here, we couple this model to a Lagrangian advection-dispersion model that tracks the movement of dissolved CO_2 in the water column and to a model of CO_2 speciation in natural seawater (the csys software[51]). Simulations provide a means to evaluate the mass flow rate at CO_2 seepage/leakage sites based on observed anomalies in seawater chemistry (e.g., pH or partial pressure of CO_2, pCO_2). The model is intended to be used as a tool for analyzing field data and to guide sampling during experimental CO_2 release experiments and field monitoring of existing and future storage sites.

METHODS

Study Site. Panarea is the smallest of the seven major islands of the Aeolian volcanic arc situated offshore northern Sicily and western Calabria (Figure 1).[29,52] The ongoing volcanic activity started ∼1.5 Ma ago in this region.[52,53] The offshore CO_2 gas seep system at Panarea has been known since historical times.[52] These emanations originate from an underground geothermal reservoir fed by a magmatic body.[36] In this near-shore setting, thermal waters and >90% pure CO_2 gas are emitted into the sea at depths ranging from < 10 m to > 300 m below the sea surface.[54,55] Early observations focused on the shallowest seepage locations (<10−20 m depth) that are located between the islets Dattilo, Panarelli, Lisca Bianca, Bottaro, and Lisca Nera.[36] Numerous emission sources range from single bubble streams[29] to stronger sources generating upward entrainment of ambient water through the formation of bubble plumes.[54] The emitted gas consists of small proportions of nitrogen (N_2), hydrogen sulfide (H_2S), helium (He), hydrogen (H_2), methane (CH_4), argon (Ar), and carbon monoxide (CO).[29,40,52,56] The seepage system around Panarea Island represents a continuous natural experiment for understanding the behavior of CO_2 emissions to the water column.[29,42]

Field Observations. During cruise POS469 (May 2−22, 2014), several CO_2 release sites offshore Panarea were visited.[43] This included a shallow site at Bottaro crater (12 m depth) accessible by scuba diving and another site termed station PCTD3 at 40−50 m depth (Figure 1). At Bottaro crater, we monitored bubble size and performed gas composition measurements based on discrete samples of gas bubbles at different depths. This data set was used to validate the TAMOC model (see below). At station PCTD3, investigations were based on continuous pH monitoring, CTD and ADCP measurements, and bathymetrical mapping.

Bottaro Crater. A scuba diving sampling campaign was conducted on May 10−19, 2014 at a shallow location (12 m depth) close to the Bottaro Islet, located ∼3 km east of Panarea.[43] The Bottaro crater is a depression resulting from a massive gas eruption in 2002.[52] Gas emission has continued to this day although at a much lower rate. The crater has a 13 × 26 m^2 oval shape and is covered by pebbles. A seepage zone consisting of more evenly distributed weaker bubble streams is present over a 13 × 17 m^2 zone at the SE end of the crater. The rim of the crater features a few more discrete and stronger vents.[57] On May 12, 2014, bubbles released within the weaker seepage field were imaged against a 2 m high white polystyrene screen acting as a diffusor for a 17,000 lm light source. Two tilted planes deployed at the seafloor permitted only bubbles directly in front of the diffusor to enter the field of view of the camera. The video included a scale with millimeter graduations (Figure S-1). A volume flow rate of 0.56 L min^{-1} at a water depth of 12 m was quantified by timing the filling of a 250 mL container held over the bubble stream. The initial bubble size distribution was determined with Matlab by manually positioning ellipses over the 194 bubbles identified within 17 video frames. The frames were selected randomly and at long time intervals to ensure that each frame contained a new, independent set of bubbles. The bubble volumes as determined from the ellipse minor and major axes were scaled to the measured volume flow rate (0.56 L min^{-1}) by assuming an average bubble slip velocity of 25 cm s^{-1},[58] and the equivalent spherical diameter was calculated.[59,60] This procedure is deemed to be a reasonable proxy for bubble volume if more advanced techniques[61,62] cannot be applied. The measured bubble size distribution was assumed to be representative of shallow seafloors in the vicinity exhibiting similar mechanical properties[16,23] (such as vent C, defined below).

A total of 26 gas samples (two at each depth) were acquired at a focused gas vent ("vent C", Figure 1) of high intensity (9.3 L min^{-1} at 12 m depth) on May 16, 2014. Hungate tubes were fixed to a vertical rope at 1 m intervals from the 12 m deep seafloor to the sea surface, where the rope was attached to a buoy. After sampling ascending gas bubbles, the Hungate tubes were closed at depth. 100 μL Subsamples were taken from the Hungate tubes and injected into a gas chromatograph (GC) onboard the R/V *Poseidon* to determine the CO_2 contents, following a previously described method.[29] Additionally, 13 water samples were taken on May 12 and 13, 2014 to determine the dissolved gas concentration within the ambient seawater. 100 mL Headspace vials were filled with seawater at 40 cm vertical intervals (0−2 m above seafloor) and subsequently crimp-sealed under water. Helium was injected into the vials in order to create a 20 mL headspace by partly removing the water via a compensation needle. To stop microbial respiration, the headspace samples were immediately poisoned by adding 20 μL of $HgCl_2$.

During sampling at vent C, the 12 m water column was observed to be vertically well-mixed as a result of a moderate gale (Bft 7) on May 14, 2014. The water temperature was 17.9 °C and salinity was 37.8 over the full 0−12 m depth interval. For this well-mixed, shallow water column, the dissolved O_2 concentration was assumed to be at equilibrium with the atmosphere (250 μmol L^{-1}). Horizontal water currents ranged from 0 to 16.2 cm s^{-1}, as measured with a SonTek Argonaut ADCP at 12 m depth at Bottaro Crater on May 15−16, 2014.

Station PCTD3. Station PCTD3 was located at a deeper gas release zone (40−50 m below the sea surface) situated ∼1 km east of Panarea (Figure 1). In this approximately 300 × 400 m^2 area, a video CTD water sampling rosette was towed from the R/V *Poseidon* to map CO_2 and to provide seafloor images. The video covered ∼12% of the seafloor surface area and revealed 294 individual bubble streams (Figure 1).

The video CTD included a SBE27−0202 pH sensor (∼0.1 accuracy, ∼0.005 resolution, 1 s response time); 1 min

DOI: 10.1021/acs.est.9b02131
Environ. Sci. Technol. 2019, 53, 10258−10268

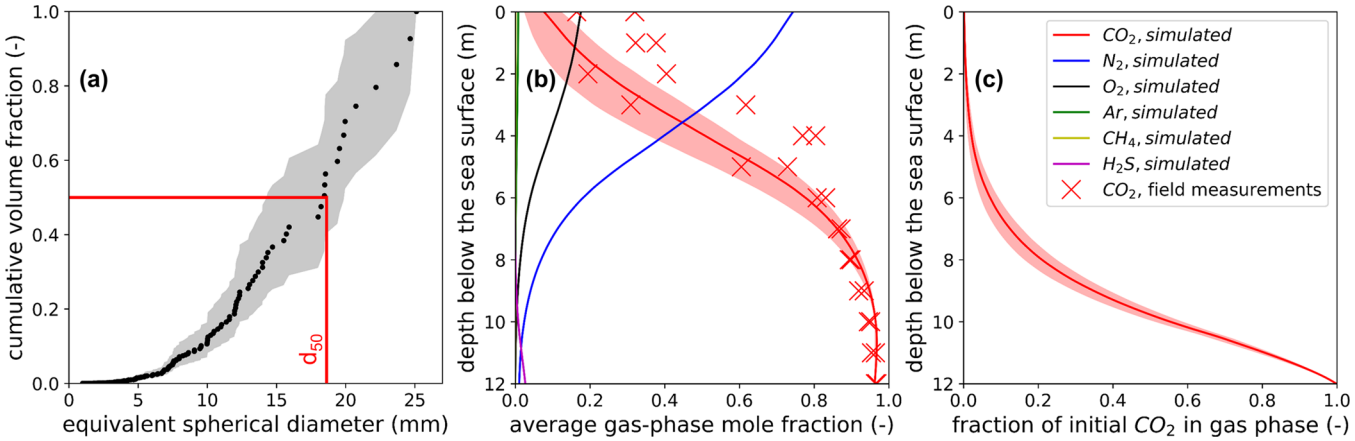

Figure 2. (a) Observed initial bubble size distribution at Bottaro crater on May 12, 2014 (solid dots) and bootstrap 95% confidence interval (gray area). (d_{50} = volume median diameter). (b) Evolving average composition of the gas phase from the emission source at a 12 m depth (vent C) to the sea surface, as predicted by TAMOC for all simulated compounds (solid lines = measured initial bubble size distribution, shaded area = 95% confidence interval as defined on panel a, displayed only for CO_2), and measured in the field for CO_2 (×). (c) Fraction of the CO_2 released at the emission source remaining within gas bubbles as a function of depth, according to the TAMOC simulation.

averaged data was used for model validation. The video CTD was operated in two separate modes: (A) the instrument was maintained within 1−2 m above seafloor, and (B) the instrument was towed at an approximately constant depth (45−48 and 37−39 m below the sea level). An ADCP was positioned by the remotely operated vehicle (ROV) PHOCA[63] upstream of station PCTD3 during the whole sampling period (Figure 1). It recorded water current velocity with a 5 min time resolution and a 1 m vertical resolution (3.22 m for the first bin above seafloor). Additional description of the field work at station PCTD3 has been presented previously.[29]

MODEL

The new model couples existing models for predicting the behavior of gaseous CO_2 released in seawater. The three parts of the new model are described below, including the near-field bubble plume model TAMOC, the Lagrangian dissolved CO_2 advection-dispersion model, and the carbonate system model csys.

TAMOC Bubble, Droplet, and Multiphase Plume Model. Dynamics of bubbles were simulated using the TAMOC model,[44−48,50] version 1.1.1. TAMOC includes a three-dimensional single-bubble model, which simulates low-intensity bubble streams (Figure 2). The bubble model was run within a bent plume model[44] to simulate cases where uplift of ambient water was generated by stronger gas releases, resulting in a bubble plume, bent horizontally by cross-flow currents. The TAMOC model (including bubble dynamics and single and multiphase plume behaviors) was previously validated based on laboratory and field data ranging from ∼1 m to 1500 m water depth. This includes 64 laboratory data sets for bubbly jets and bubble plumes in quiescent conditions, stratified stagnant conditions, and crossflow conditions, as well as field data from the *DeepSpill* gas and oil release experiment, the 2010 *Deepwater Horizon* oil spill, and natural gas seep data.[44−48,50,64,65]

TAMOC solves for mass transfer of CO_2, other emitted gases, and major seawater gases (here: N_2, O_2, and Ar) across the bubble−water interface, three-dimensional bubble trajectories, as well as bubble size evolution as a function of evolving total bubble mass, pressure, temperature, and composition.[44,46] The model includes a real-fluid equation of state[66,67] and is able to predict densities[66−68] and solubilities[69−72] of gas and liquid mixtures at the range of pressure, temperature, and salinity conditions present in global oceans (≤10,000 m water depth, salinity of ∼35, temperatures of −2 to 30 °C).[47] The bent plume model additionally solves for entrainment of ambient water, conservation of momentum, heat, and salt.[44] It also predicts separation positions at which bubbles of different sizes exit the plume, and terminates the plume simulation where the plume water detrains due to stratification. Thereupon, gas bubbles are assumed to behave independently from each other, and they are simulated until they either fully dissolve or reach the sea surface. Differential equations are solved using the backward differentiation formula of the VODE method[73] of the "integrate" Python package with adaptive step size, designed for stiff equations.

Mass transfers are calculated according to[74]

$$\frac{dm_i}{dt} = -A \times \beta_i \times (C_{w,i}^{eq} - C_{w,i}) \quad (1)$$

where m_i is the total mass of compound i in the bubble, A is the surface area of the bubble, β_i is the mass transfer coefficient (units: length time^{-1}) of compound i at the gas−water interface, $C_{w,i}^{eq}$ is the equilibrium aqueous concentration of compound i; and $C_{w,i}$ is the modeled aqueous concentration of compound i in the seawater adjacent to the bubble. Values of C_w in the buoyant plume are computed from the volume of water present in the corresponding water mass at that location and the simulated dissolved mass. Properties of bubbles, including shape, surface area, slip velocity, and β_i, are estimated based on published formulas,[58,75] as explained previously.[46]

Gas bubbles are observed to exhibit either circulating or noncirculating interfaces depending on conditions.[58,74,76] A circulating interface leads to more rapid mass transfers because of the convection brought by the free movement at the interface. In the presence of natural or manmade surfactants, these would accumulate at the interface, which would be immobilized (noncirculating), leading to slower mass transfer across the gas−water interface. We simulated circulating bubble interfaces in agreement with assumptions made by previous studies for gas bubbles in the sea[13,16,17,23,25,77−79] (see also the Supporting Information, sections S-2 and S-10).

DOI: 10.1021/acs.est.9b02131
Environ. Sci. Technol. 2019, 53, 10258−10268

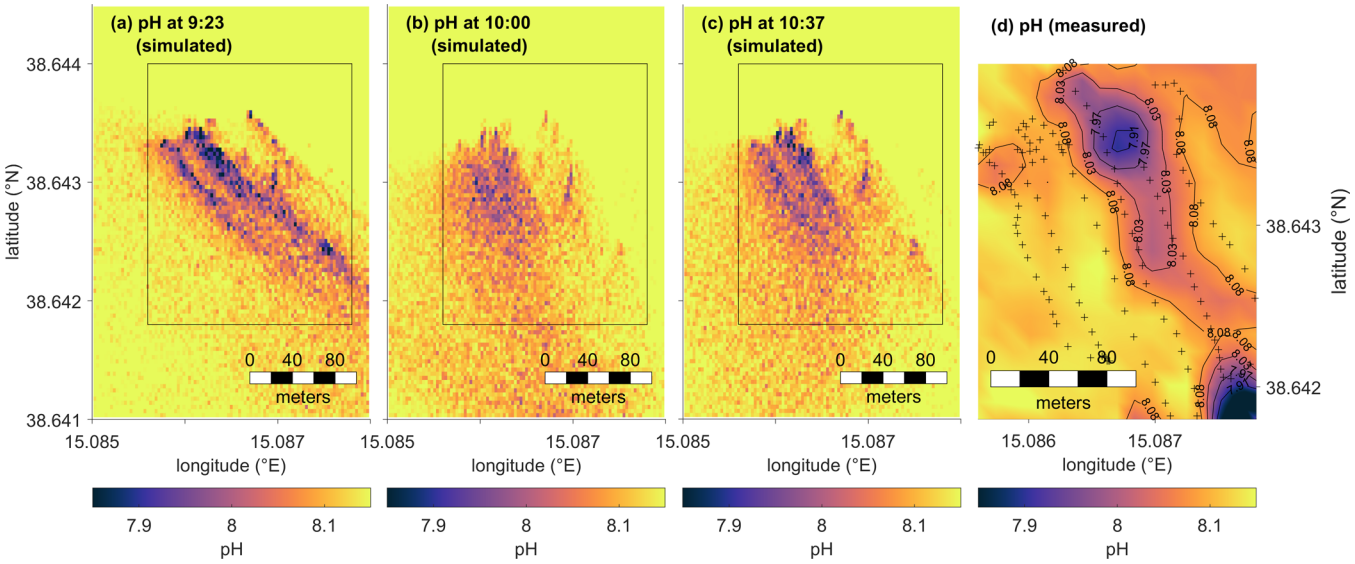

Figure 3. (a–c) Simulated pH map at three time points on May 8, 2014 and (d) observed map of pH calculated for May 8, 2014 at 8:45–11:15 am, at 1–2 m above the seafloor (panels a–d). (d) The map was generated from measured data ("+" symbols) using ordinary kriging as implemented in the EasyKrig Matlab software (version 3.0, Dezhang Chu and Woods Hole Oceanographic Institution, downloaded from ftp://globec.whoi.edu/pub/software/kriging/easy_krig/V3.0.2-Matlab2016b/ on Jan 28, 2019); based on the variogram, the following parameters were used. Model: general exponential-Bessel, nugget: 0, sill: 1, length: 0.15, power: 2, hole scl: 0, range: 0.95. The reader is referred to Movie S-1 for model predictions at a 10 s time step interval. The spatial extent covered by panel (d) is indicated on panels (a–c) by a black rectangle.

The interfacial tension between the seawater and gas bubbles was assumed equal to the surface tension of seawater at ambient conditions. The profile of O_2 concentrations in the water column was measured. Additionally, it was assumed that N_2 and Ar concentrations were at atmospheric saturation, which corresponds within a few percent to observations in Earth oceans under normal oxic conditions.[74,80,81] Other gases were assumed initially absent from ambient seawater for the purpose of mass transfer calculations (including CO_2). The impact of dissolved CO_2 on seawater density is negligible at the levels observed in the field (section S-3).

For Bottaro Crater, simulations of CO_2 assumed a constant horizontal water current of 5 cm s^{-1} (within the range of measured values), and an emission source diameter of 10 cm at the seafloor (based on field observations). Composition of the gas released at the seafloor was based on the observed average composition measured (96.2 ± 2.3% CO_2, 1.1 ± 0.3% N_2, 0.0014 ± 0.0001% CH_4, and 2.7 ± 2.2% H_2S at Bottaro Crater, under the assumptions explained in Table S-2).

Dissolved CO_2 Lagrangian Advection-Dispersion Model. Simulation of the fate of aqueous CO_2 uses a Lagrangian advection and a random-walk model, similar to previous studies of CO_2 releases in the sea[17,82] and dissolved chemicals during oil spills.[83] In a Lagrangian model,[84] the continuous concentration field is simulated by tracking discrete Lagrangian parcels of dissolved CO_2 having a three-dimensional position and infinitesimal size. Integration of millions of tracked Lagrangian parcels over an Eulerian grid of cells provides the concentration field at chosen time points.[84] The near-field bubble (plume) simulation is performed online with TAMOC, providing the 3D mass flow rate of dissolved CO_2 entering the sea as a function of time and position above each simulated emission site which depends on the instantaneous measured water velocity field (assumed constant over the spatial model domain and interpolated from ADCP measurements performed at 5 min intervals). At each simulated emission source (Figure 1), the input of dissolved CO_2 to the water column from ascending bubbles is discretized in ten vertical bins. A Lagrangian parcel of dissolved CO_2 is released for each bin at each time step, and they subsequently move according to

$$\Delta x = U_E \times \Delta t + \text{rand} \times \sqrt{2 \times D_x \times \Delta t} \quad (2)$$

$$\Delta y = U_N \times \Delta t + \text{rand} \times \sqrt{2 \times D_y \times \Delta t} \quad (3)$$

$$\Delta z = \text{rand} \times \sqrt{2 \times D_z \times \Delta t} \quad (4)$$

where Δx, Δy, and Δz are the displacements of a parcel over one time step in the x (east), y (north), and z (vertical) directions, respectively; Δt is the time step (10 s for station PCTD3, section S-5); rand is a normally distributed random number having a mean of 0 and standard deviation of 1; U_E and U_N are the ADCP water current velocities at the time and depth of interest in the east and north directions, respectively; and D_x, D_y, and D_z are the turbulent diffusion coefficients in the x, y, and z directions. The seafloor and sea surface are simulated as reflective wall boundaries.[85,86] The implementation of the Lagrangian advection-dispersion model is validated with the analytical solution for a point source in section S-6.

Contrary to Eulerian models, concentrations predicted by Lagrangian, random-walk models are somewhat dependent on the grid resolution. However, we consider that this is balanced by the fact that Lagrangian models do not suffer from numerical diffusion and stability issues that are common to Eulerian models.

At time points of interest, excess dissolved inorganic carbon concentrations (excess DIC) relative to the background signal observed in the field (2.269 mmol kg^{-1}, fitted to the pH measurements above the 95% percentile) were calculated by integration of the mass of the Lagrangian parcels over a spatial grid[84] (~300 × 400 m^2 in size, Figure 3). For simulations at station PCTD3, cells were defined as having a 1 m height and 2.6–3.9 m width in east and north directions, respectively. The

DOI: 10.1021/acs.est.9b02131
Environ. Sci. Technol. 2019, 53, 10258–10268

chosen cell size is a trade-off between resolution and the number of parcels of dissolved CO_2 that could be tracked without reaching the computer memory limit (16 GB of RAM). To decrease the memory requirement, particles exiting the spatial range plotted on Figure 3a−c by more than 50 m distance were immediately "forgotten" by the Lagrangian model, which simultaneously tracked a total of ∼2 × 10^6 parcels within the simulated domain. Simulations at Station PCTD3 used $D_x = D_y = 10^{-2}$ m^2 s^{-1} (based on Okubo's diagram[86,87]), and $D_z = 10^{-3}$ m^2 s^{-1} (based on a value selected for the energetic sea-surface upper 40-m layer,[83] in good agreement with values selected in other studies[17]).

For simulations at station PCTD3, the positions of the observed bubble streams (Figure 1) were used to initiate the bubble releases within the simulations. Bubbles were assumed to exit the seafloor with initial diameters following a size distribution measured at station PCTD3 (section S-7), and the seafloor was assumed to have a constant depth of 51.22 m, neglecting local bathymetry variation. Because the observed bubble streams were weak at station PCTD3, the TAMOC simulations were run with the single bubble model (absence of bubble plumes assumed). Finally, the aqueous dissolution of CO_2 within the seafloor[15,88] and the subsequent flux of dissolved CO_2 species through the sediment−water interface was considered negligible. Previous investigations in the immediate vicinity of our study site by Molari et al.[89] (East of Basiluzzo Islet, June 1−14, 2013) indicate that the measured flux of gaseous CO_2 (253−317 mol m^{-2} d^{-1}) was 34−57× larger than the average flux of dissolved CO_2 species (DIC) through the sediment water interface (5.5−7.4 mol m^{-2} d^{-1}).[89]

Carbonate Model. Finally, the pCO_2 and the pH change was obtained for each cell by calculating the equilibrium marine carbonate system using the csys Matlab software (https://www.soest.hawaii.edu/oceanography/faculty/zeebe_files/CO2_System_in_Seawater/csys.html, section S-8). The csys software calculates the equilibrium partitioning of the carbon dioxide and related chemical species in seawater (CO_2, HCO_3^-, CO_3^{2-}, etc.) and the resulting pH. Input parameters to the csys software include the total DIC (background DIC + excess DIC), total alkalinity (2.600 mmol kg^{-1} [90]), temperature, pressure, and salinity. Csys follows a procedure based on that described by Zeebe and Wolf-Gladrow,[51] and it performs similarly to nine other models of the carbonate system.[91]

Code Implementation. TAMOC is a freely available software implemented in Python and Fortran (https://github.com/socolofs/tamoc/), with the user interacting with the model from the Python side. The particle-tracking algorithm was implemented in Matlab, interfaced with Python so that TAMOC can be called directly from the Lagrangian advection-dispersion model. The csys model is also coded in Matlab and was interfaced with our algorithms as described in Section S-8.

Estimate of Total Gas Flow Rate at Station PCTD3. Assuming an equal mass flow rate at each of the 294 simulated emission sources, dissolved concentrations were predicted as a function of the total mass flow rate over the studied area. The mass flow rate leading to the lowest root mean squared deviation (RMSD) between pH field observations and simulations was selected as the best estimate. Simulated values were calculated within a vertical cylinder of 10 m radius, extending 1−2 m from the seafloor, at the time and location of corresponding field observations, coherent with the resolution of field measurements.

RESULTS & DISCUSSION

Bottaro Crater. Bubbles at the weaker seepage area at Bottaro crater had a volume median diameter (d_{50}) of 18.4 mm, with a bootstrap 95% confidence interval of 14.3−19.9 mm (Figure 2a). This confidence interval was determined by 10,000 bootstrap resampling of the observed size distribution.[92] 6% of the bubbles carried 50% of the released gas, with >50% of the bubble number (<5 mm) contributing <1.5% to the released volume. The observed d_{50} is larger than most previous field observations at 10−2870 m depth,[23,34,62,76,93−97] but not unprecedented,[98] which might be related to the particular setting at Bottaro crater where the seafloor is covered with centimeter-sized pebbles.

A fluorescein dye injection experiment that we performed at vent C highlighted the formation of a bubble plume (Figure S-10). Vent C was therefore simulated using the bent plume model in TAMOC. Simulations using the bubble size distribution observed within the weaker seepage area indicate good agreement with field measurements of the decreasing CO_2 mole fraction within gas bubbles from the seafloor to the sea surface (Figure 2b). It must be emphasized that these simulations do not require any parameter tuning, they are based on the underlying chemical and physical processes parametrized based on observed field conditions, including the measured CO_2 flow rate. This result implies that 79 ± 4% of the dissolved CO_2 input to the water column occurred within 4 m from the seafloor (Figure 2c) within this weak CO_2 bubble plume with bubbles having large initial diameters at the emission source. 99.82% of the CO_2 gas flow rate at the seafloor dissolved during the 12 m ascent in the water column and only 0.18% reached the sea surface within gas bubbles. This confirms previous findings that gaseous CO_2 is mostly dissolved within a few meters above the emission source,[13,20] resulting in much more localized inputs to the water column compared to hydrocarbon gases[13,23,46,74,76] or CO_2 droplets.[50,99,100] The results in Figure 2, panels b and c, might appear contradictory at first because most of the CO_2 escapes the ascending bubbles (Figure 2c) before a significant decrease of the CO_2 gas-phase mole fraction becomes evident (Figure 2b). This is caused by the larger solubility of CO_2, by a factor of 25−62, with respect to other major dissolved gases at local conditions. Hence, CO_2 and H_2S, which is a factor of 3 more soluble than CO_2, experience much faster mass transfer than the other gases. Additionally, the agreement between field observations and simulations in Figure 2b strongly indicates that the bubbles had circulating interfaces (Section S-10). Measured aqueous-phase pCO_2 values were ≤ 22,200 ppm at 0−2 m above the seafloor, or ≤ 1% of the saturation aqueous solubility of CO_2 (∼2.2 × 10^6 ppm at 12 m depth). Simulations confirmed that the contribution of the dissolved CO_2 on mass transfer rates was negligible (not shown).

STATION PCTD3

Estimate of Total CO_2 Mass Flow Rate. Globally, simulations predict a plume of lower pH than the surrounding water that agrees with field observations (Figures 3 and S-12b). However, simulations do not exactly reproduce the observed spatial extent of the plume, which tends to be oriented in parallel with topographic isobaths. This is likely the result of model simplifications, such as neglecting the local topography. The ADCP was located ∼200 m upstream of station PCTD3, and a COMSOL simulation indicated that the local top-

DOI: 10.1021/acs.est.9b02131
Environ. Sci. Technol. 2019, 53, 10258−10268

ography (i.e., raised seafloor toward Panarea on the west, Figure 1) is likely to have deflected incoming southward-pointing water current 12° to the east (Section S-12), in agreement with the general direction highlighted by field observations (Figure 3d). Additionally, our observations covered only ∼12% of the seafloor in the emitting area, leading to uncertain spatial distribution of emission sources. Here, we consider that the ability of the model to predict an overall similar pattern of a depressed pH plume is sufficient to provide an order-of-magnitude estimate of the total CO_2 release at station PCTD3.

The estimated total CO_2 mass flow rate at station PCTD3 is 0.22 kg s^{-1} of gas or 6900 t y^{-1} (Figures 3, S-12, S-14, and S-15). This corresponds to the average annual greenhouse gas emissions of 590 German citizens (expressed in CO_2-equivalents).[101] The estimated total CO_2 mass flow rate at station PCTD3 corresponds to 2100−9400 bubble streams, assuming single-flare volume flow rates of 0.125−0.556 L min^{-1} [29,43] (0.23−1.1 × 10^{-4} kg s^{-1} at emission depth). This is in close agreement with the 294 bubble streams observed over an estimated 12% of the whole seep area (extrapolated to ∼2500 bubble streams in total).

The offshore natural gas seepage at Panarea Island is characterized by several hotspots where seepage occurs over a total area of > 10 km^2, many at depths > 20 m.[54] Station PCTD3 is one of several seepage hotspots. The total mass flow rate estimate presented here for station PCTD3 is of the same magnitude as the total value of 9000 m^3 d^{-1} previously reported for the readily accessible 0−20 m depth release sites at Panarea[36] (0.16 kg s^{-1} at standard conditions of temperature and pressure). Consequently, these results suggest that the release sites at > 20 m water depth may represent the dominant contributors of gaseous emissions offshore Panarea Island. The poorly studied emission sites situated at water depths > 20 m therefore deserve further attention and must be included in future studies aiming at establishing global budgets of geogenic gas emissions offshore Panarea Island.

Monitoring of dissolved CO_2 levels (e.g., through in situ pCO_2 or pH measurements) is a relatively straightforward survey technique. However, model simulations are necessary for relating observations to seafloor emission rates. Our simulations highlight that the plumes of dissolved CO_2 are dynamic features that evolve within short timeframes (<15 min) under variable current forcings (Movie S-1). Sampling of an area of 1−10 × 10^4 m^2 usually requires several hours, and therefore models provide the necessary framework to understand the evolving dynamics during sampling.

Detectability of CO_2 Leaks. Identifiable pCO_2 and pH levels relative to the background are predicted only in the immediate vicinity of the seafloor (Figures 3 and 4) for the multiple, distributed emission sources at station PCTD3, with 99% of the aqueously dissolved CO_2 remaining within 10 ± 2 m from the seafloor according to simulations. Simulations predict that the pH values at 5−6 m above seafloor are close to background levels (Figure S-16), and this is confirmed by the field measurements performed at constant depth away from the seafloor (mean pH of 8.14 with a standard deviation of 0.05). This results from the high solubility of CO_2, whereby > 90% (> 99%) is predicted to dissolve within 4 (7) m of the seafloor at station PCTD3. These outcomes are principally dependent on the initial bubble size at the emission source. Despite the recent developments in models able to predict initial bubble sizes above orifices of known diameters,[16,102−104]

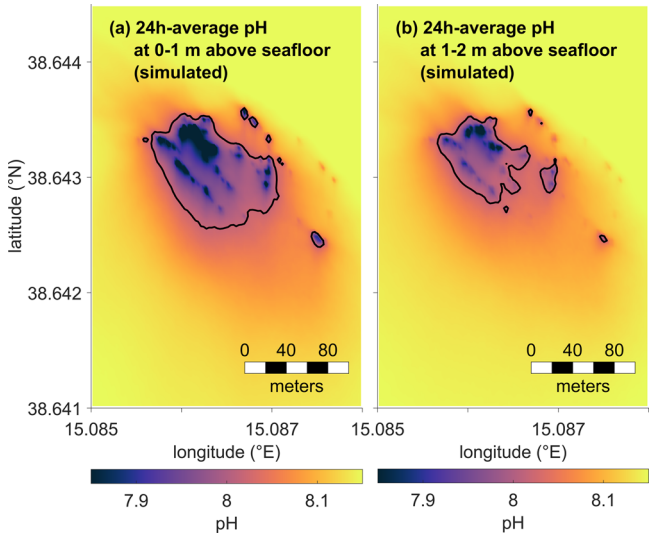

Figure 4. Average pH over a 24 h period (May 8−9, 2014, from 8 am to 8 am), at (a) 0−1 m and (b) 1−2 m above the seafloor. The solid black line indicates the potential impact limit (ΔpH = 0.15).

it remains currently impossible to precisely predict the expected bubble sizes for releases through the sediment−water interface at potential failed storage sites.[16] We therefore advise that future monitoring strategies should carefully monitor the bottom waters as closely as technically possible (ideally within 1−2 m). In case of a single emission point, the plume is expected to be narrow (<10 m width) and to change location with water currents[20] (Movie S-1). For a towed instrument, we suggest a maximum towing speed of 0.3 knots, equivalent to a spatial resolution of 5−10 m, because of sensor response times that are typically on the order of 30−60 s for pCO_2.[29] The new model presented here could be used to guide sampling strategy during CO_2 storage monitoring campaigns or monitoring of other accidental or intended gaseous releases in the marine environment.

Potential Local Environmental Impacts. Simulated predictions at station PCTD3 are taken as an indication of potential local CO_2 impacts assuming the leaks occur in an undisturbed, pristine environment. Here, changes in pH are assumed to dominate the potential impacts on the local ecosystem in the vicinity of a leak from a storage facility, neglecting the role of CO_2 itself in observed toxicity.[1] Previous studies[19,20,105] have argued that environmental impacts are unlikely when the acidification remains below the range of natural variation of pH over the year (assumed <0.15 pH units based on data for the North Sea[20]). Drops in pH (ΔpH) from 0.2−0.5 pH units have been termed potentially harmful, with ΔpH ≥ 1 pH units identified as significantly harmful.[20] Observations at Panarea Island have reported quantitative and qualitative differences in ecosystem structures at seep sites relative to unaffected sites (ΔpH of 0.1−0.6), including a 4.5-fold increase in microphytobenthos productivity and a 5-fold decrease in faunal biomass linked with decreased diversity.[89,106] Future ocean acidification resulting from the rising CO_2 atmospheric concentrations may drastically alter the carbonate cycle in world oceans (possibly decreased precipitation of carbonate minerals), potentially leading to major environmental community shifts involving calcifying organisms.[107−110]

DOI: 10.1021/acs.est.9b02131
Environ. Sci. Technol. 2019, 53, 10258−10268

On a 24 h average basis, an area of 3900 m^2 experiences a ΔpH of ≥ 0.2 pH units (Figure 4), calculated for the 0−1 m bottom water layer, with a rapid decrease of the impacted area at shallower depths (1200 m^2 at 1−2 m above seafloor). On an instantaneous basis, ΔpH can reach up to 2.2 pH units locally, with a maximum area of 6300 m^2 experiencing significantly harmful pH drops (ΔpH ≥ 1). During the 24 h period shown in the figure, an average area of 600 m^2 (standard deviation: 1300 m^2) experienced ΔpH ≥ 1 at any given time. The pH varied over short time scales as a function of time-varying water currents (Movie S-1), and this result may depend on the period within a 28-day tidal cycle. It is likely that marine organisms can survive acute exposure to ΔpH values of this magnitude,[1] and we hypothesized that the 24 h average ΔpH is likely representative of the chronic exposure level.

These local estimates must also be considered in the context of ongoing anthropogenic CO_2 emissions: the pH of world oceans is predicted to decrease by up to 0.4 pH units by the end of the 21st century relative to the preindustrial level.[3,111] As a consequence, the local impacts faced by marine communities near such leakages (≤ 1.9 × 10^{-2} km^2 experiencing ΔpH ≥ 0.5) would be dwarfed by a change of similar magnitude in the surface waters of world oceans (361 × 10^6 km^2).[71]

■ ASSOCIATED CONTENT

Supporting Information

The Supporting Information is available free of charge on the ACS Publications website at DOI: 10.1021/acs.est.9b02131.

Description of the bubble parametrization rack; TAMOC example validation; effect of CO_2 on seawater density; composition of emitted gas at station PCTD3 and Bottaro Crater; sensitivity of the Lagrangian advection-dispersion model to the time step; validation of the Lagrangian advection-dispersion model; initial bubble size distribution at station PCTD3; carbonate system model; fluorescein release experiment; simulation at vent C assuming noncirculating bubble interfaces; validation of model simulation with individual pH measurements; COMSOL Multiphysics simulation of water currents at station PCTD3; model predictions for low and high gas flow rates at station PCTD3; and model predictions for 5−6 m above the seafloor at station PCTD3 (PDF)

4 h Movie (May 8, 8 am to May 9, 8 am) of predicted pCO_2 and pH at both 0−1 and 1−2 m above the seafloor displayed in four panels (AVI)

■ AUTHOR INFORMATION

Corresponding Author

*Phone: +49 431 600-2267; e-mail: jogros@geomar.de.

ORCID

Jonas Gros: 0000-0002-2237-9168

Present Address

‡Geotek, 3 Faraday Close, Daventry Northamptonshire NN11 8RD, United Kingdom.

Notes

The authors declare no competing financial interest.

■ ACKNOWLEDGMENTS

We thank Captain Klaus Ricke, his crew, the GEOMAR ROV team, and Sergiy Cherednichenko for support provided during the R/V *Poseidon* cruise, Amphibia Diving Center Panarea, Matthias Kreuzburg and Christian Howe (scuba divers), and the GEOMAR technology and logistics center for logistic support. The cruise and diving campaign has received funding from GEOMAR, the Helmholtz-Alliance "ROBEX − Robotic Exploration of Extreme Environments", the ECO2 project in the European Community's Seventh Framework Program (FP7/2007-2013) under grant agreement n° 265847, and 3 mini projects funded by the cluster of excellence "The Future Ocean". This project has received funding from the European Union's Horizon 2020 research and innovation programme under grant agreement no. 654462 STEMM-CCS.

■ REFERENCES

(1) IPCC. *Carbon Dioxide Capture and Storage: Special Report of the Intergovernmental Panel on Climate Change*, Intergovernmental Panel on Climate Change.; Cambridge University Press: New York, 2005.

(2) IPCC. *Global Warming of 1.5 °C, An IPCC Special Report on the Impacts of Global Warming of 1.5 °C above Pre-Industrial Levels and Related Global Greenhouse Gas Emission Pathways, in the Context of Strengthening the Global Response to the Threat of Climate Change, Sustainable Development, and Efforts to Eradicate Poverty, Summary for Policymakers*; IPCC SR 1.5; IPCC: Geneva, Switzerland, 2018; p 33.

(3) Edenhofer, O.; Pichs-Madruga, R.; Sokona, Y.; Minx, J.; Farahani, E.; Kadner, S.; Seyboth, K.; Adler, A.; Baum, I.; Brunner, S.; et al. *IPCC, 2014: Climate Change 2014: Mitigation of Climate Change. Contribution of Working Group III to the Fifth Assessment Report of the Intergovernmental Panel on Climate Change*; Cambridge University Press: Cambridge (UK) and New York (USA), 2014.

(4) Holloway, S. Storage of Fossil Fuel-Derived Carbon Dioxide beneath the Surface of the Earth. *Annu. Rev. Energy Environ.* **2001**, *26* (1), 145−166.

(5) Vangkilde-Pedersen, T.; Vosgerau, H.; Willscher, B.; Neele, F.; van der Meer, B.; Bossie-Codreanu, D.; Wojcicki, A.; Le Nindre, Y.-M.; Kirk, K.; von Dalwigk, I.; et al. *Capacity Standards and Site Selection Criteria*; EU GeoCapacity WP4 report; 2009; p 48.

(6) EU GeoCapacity. Assessing European Capacity for the Geological Storage of Carbon Dioxide. *D16, WP2 Report, Storage Capacity*; 2009; p 170.

(7) *CO_2 Storage Atlas Norwegian North Sea*; Norwegian Petroleum Directorate: Stavanger, Norway, p 72.

(8) Eiken, O.; Ringrose, P.; Hermanrud, C.; Nazarian, B.; Torp, T. A.; Høier, L. Lessons Learned from 14 Years of CCS Operations: Sleipner, In Salah and Snøhvit. *Energy Procedia* **2011**, *4*, 5541−5548.

(9) Karstens, J.; Ahmed, W.; Berndt, C.; Class, H. Focused Fluid Flow and the Sub-Seabed Storage of CO_2: Evaluating the Leakage Potential of Seismic Chimney Structures for the Sleipner CO_2 Storage Operation. *Mar. Pet. Geol.* **2017**, *88*, 81−93.

(10) Goodman, A.; Sanguinito, S.; Levine, J. S. Prospective CO_2 Saline Resource Estimation Methodology: Refinement of Existing US-DOE-NETL Methods Based on Data Availability. *Int. J. Greenhouse Gas Control* **2016**, *54*, 242−249.

(11) Directive 2009/31/EC of the European Parliament and of the Council of 23 April 2009 on the Geological Storage of Carbon Dioxide and Amending Council Directive 85/337/EEC, European Parliament and Council Directives 2000/60/EC, 2001/80/EC, 2004/35/EC, 2006/12/EC, *2008/1/EC and Regulation (EC) No 1013/2006*; 2009.

(12) *Best Practices for: Site Screening, Site Selection, and Initial Characterization for Storage of CO_2 in Deep Geologic Formations*; U.S. Department of Energy, National Energy Technology Laboratory, 2013.

(13) McGinnis, D. F.; Schmidt, M.; DelSontro, T.; Themann, S.; Rovelli, L.; Reitz, A.; Linke, P. Discovery of a Natural CO_2 Seep in the

DOI: 10.1021/acs.est.9b02131
Environ. Sci. Technol. 2019, 53, 10258−10268

German North Sea: Implications for Shallow Dissolved Gas and Seep Detection. *J. Geophys. Res.* **2011**, *116* (C3), DOI: 10.1029/2010JC006557.
(14) Monastersky, R. Seabed Scars Raise Questions over Carbon-Storage Plan. *Nature* **2013**, *504* (7480), 339.
(15) Roberts, J. J.; Stalker, L. What Have We Learned about CO_2 Leakage from Field Injection Tests? *Energy Procedia* **2017**, *114*, 5711−5731.
(16) Dewar, M.; Wei, W.; McNeil, D.; Chen, B. Small-Scale Modelling of the Physiochemical Impacts of CO_2 Leaked from Sub-Seabed Reservoirs or Pipelines within the North Sea and Surrounding Waters. *Mar. Pollut. Bull.* **2013**, *73* (2), 504−515.
(17) Dissanayake, A. L.; DeGraff, J. A.; Yapa, P. D.; Nakata, K.; Ishihara, Y.; Yabe, I. Modeling the Impact of CO_2 Releases in Kagoshima Bay, Japan. *J. Hydro-Environ. Res.* **2012**, *6* (3), 195−208.
(18) Hvidevold, H. K.; Alendal, G.; Johannessen, T.; Ali, A.; Mannseth, T.; Avlesen, H. Layout of CCS Monitoring Infrastructure with Highest Probability of Detecting a Footprint of a CO_2 Leak in a Varying Marine Environment. *Int. J. Greenhouse Gas Control* **2015**, *37*, 274−279.
(19) Phelps, J. J. C.; Blackford, J. C.; Holt, J. T.; Polton, J. A. Modelling Large-Scale CO_2 Leakages in the North Sea. *Int. J. Greenhouse Gas Control* **2015**, *38*, 210−220.
(20) Vielstädte, L.; Linke, P.; Schmidt, M.; Sommer, S.; Haeckel, M.; Braack, M.; Wallmann, K. Footprint and Detectability of a Well Leaking CO_2 in the Central North Sea: Implications from a Field Experiment and Numerical Modelling. *Int. J. Greenhouse Gas Control* **2019**, *84*, 190−203.
(21) Leifer, I. Seabed Bubble Flux Estimation by Calibrated Video Survey for a Large Blowout Seep in the North Sea. *Mar. Pet. Geol.* **2015**, *68*, 743−752.
(22) Sommer, S.; Schmidt, M.; Linke, P. Continuous Inline Mapping of a Dissolved Methane Plume at a Blowout Site in the Central North Sea UK Using a Membrane Inlet Mass Spectrometer − Water Column Stratification Impedes Immediate Methane Release into the Atmosphere. *Mar. Pet. Geol.* **2015**, *68*, 766−775.
(23) Vielstädte, L.; Karstens, J.; Haeckel, M.; Schmidt, M.; Linke, P.; Reimann, S.; Liebetrau, V.; McGinnis, D. F.; Wallmann, K. Quantification of Methane Emissions at Abandoned Gas Wells in the Central North Sea. *Mar. Pet. Geol.* **2015**, *68*, 848−860.
(24) Vielstädte, L.; Haeckel, M.; Karstens, J.; Linke, P.; Schmidt, M.; Steinle, L.; Wallmann, K. Shallow Gas Migration along Hydrocarbon Wells−An Unconsidered, Anthropogenic Source of Biogenic Methane in the North Sea. *Environ. Sci. Technol.* **2017**, *51* (17), 10262−10268.
(25) Beaubien, S. E.; De Vittor, C.; McGinnis, D. F.; Bigi, S.; Comici, C.; Ingrosso, G.; Lombardi, S.; Ruggiero, L. Preliminary Experiments and Modelling of the Fate of CO_2 Bubbles in the Water Column Near Panarea Island (Italy). *Energy Procedia* **2014**, *59*, 397−403.
(26) Schulze, G.; Schlünder, E. U. Physical Absorption of Single Gas Bubbles in Degassed and Preloaded Water. *Chem. Eng. Process.* **1985**, *19* (1), 27−37.
(27) Dewar, M.; Sellami, N.; Chen, B. Dynamics of Rising CO_2 Bubble Plumes in the QICS Field Experiment: Part 2 − Modelling. *Int. J. Greenhouse Gas Control* **2015**, *38*, 52−63.
(28) Atamanchuk, D.; Tengberg, A.; Aleynik, D.; Fietzek, P.; Shitashima, K.; Lichtschlag, A.; Hall, P. O. J.; Stahl, H. Detection of CO_2 Leakage from a Simulated Sub-Seabed Storage Site Using Three Different Types of pCO_2 Sensors. *Int. J. Greenhouse Gas Control* **2015**, *38*, 121−134.
(29) Schmidt, M.; Linke, P.; Sommer, S.; Esser, D.; Cherednichenko, S. Natural CO_2 Seeps Offshore Panarea: A Test Site for Subsea CO_2 Leak Detection Technology. *Mar. Technol. Soc. J.* **2015**, *49* (1), 19−30.
(30) Enting, I. G.; Etheridge, D. M.; Fielding, M. J. A Perturbation Analysis of the Climate Benefit from Geosequestration of Carbon Dioxide. *Int. J. Greenhouse Gas Control* **2008**, *2* (3), 289−296.
(31) Haugan, P. M.; Joos, F. Metrics to Assess the Mitigation of Global Warming by Carbon Capture and Storage in the Ocean and in Geological Reservoirs. *Geophys. Res. Lett.* **2004**, *31* (18), 1−4.
(32) Shaffer, G. Long-Term Effectiveness and Consequences of Carbon Dioxide Sequestration. *Nat. Geosci.* **2010**, *3* (7), 464−467.
(33) Blackford, J. C.; Kita, J. A Novel Experimental Release of CO_2 in the Marine Environment to Aid Monitoring and Impact Assessment. *Energy Procedia* **2013**, *37*, 3387−3393.
(34) Sellami, N.; Dewar, M.; Stahl, H.; Chen, B. Dynamics of Rising CO_2 Bubble Plumes in the QICS Field Experiment: Part 1 − The Experiment. *Int. J. Greenhouse Gas Control* **2015**, *38*, 44−51.
(35) Botnen, H. A.; Omar, A. M.; Thorseth, I.; Johannessen, T.; Alendal, G. The Effect of Submarine CO_2 Vents on Seawater: Implications for Detection of Subsea Carbon Sequestration Leakage. *Limnol. Oceanogr.* **2015**, *60* (2), 402−410.
(36) Italiano, F.; Nuccio, P. M. Geochemical Investigations of Submarine Volcanic Exhalations to the East of Panarea, Aeolian Islands, Italy. *J. Volcanol. Geotherm. Res.* **1991**, *46* (1), 125−141.
(37) Lupton, J.; Lilley, M.; Butterfield, D.; Evans, L.; Embley, R.; Massoth, G.; Christenson, B.; Nakamura, K.-I.; Schmidt, M. Venting of a Separate CO_2-rich Gas Phase from Submarine Arc Volcanoes: Examples from the Mariana and Tonga-Kermadec Arcs. *J. Geophys. Res.* **2008**, *113*, B08S12.
(38) Roberts, J. J.; Wilkinson, M.; Naylor, M.; Shipton, Z. K.; Wood, R. A.; Haszeldine, R. S. Natural CO_2 Sites in Italy Show the Importance of Overburden Geopressure, Fractures and Faults for CO_2 Storage Performance and Risk Management. *Geol. Soc. Spec. Publ.* **2017**, *458*, 181.
(39) Gugliandolo, C.; Italiano, F.; Maugeri, T. The Submarine Hydrothermal System of Panarea (Southern Italy): Biogeochemical Processes at the Thermal Fluids - Sea Bottom Interface. *Ann. Geophys.* **2006**, *49* (2−3), DOI: 10.4401/ag-3139.
(40) Inguaggiato, S.; Diliberto, I. S.; Federico, C.; Paonita, A.; Vita, F. Review of the Evolution of Geochemical Monitoring, Networks and Methodologies Applied to the Volcanoes of the Aeolian Arc (Italy). *Earth-Sci. Rev.* **2018**, *176*, 241−276.
(41) Esposito, V.; Andaloro, F.; Canese, S.; Bortoluzzi, G.; Bo, M.; Bella, M. D.; Italiano, F.; Sabatino, G.; Battaglia, P.; Consoli, P.; et al. Exceptional Discovery of a Shallow-Water Hydrothermal Site in the SW Area of Basiluzzo Islet (Aeolian Archipelago, South Tyrrhenian Sea): An Environment to Preserve. *PLoS One* **2018**, *13* (1), e0190710.
(42) Caramanna, G.; Voltattorni, N.; Maroto-Valer, M. M. Is Panarea Island (Italy) a Valid and Cost-Effective Natural Laboratory for the Development of Detection and Monitoring Techniques for Submarine CO_2 Seepage? *Greenhouse Gases: Sci. Technol.* **2011**, *1* (3), 200−210.
(43) *RV POSEIDON Fahrtbericht/Cruise Report POS469*; Linke, P. and shipbord scientific party, Eds.; 19; GEOMAR: Kiel, 2014.
(44) Dissanayake, A. L.; Gros, J.; Socolofsky, S. A. Integral Models for Bubble, Droplet, and Multiphase Plume Dynamics in Stratification and Crossflow. *Environ. Fluid Mech.* **2018**, *18*, 1167.
(45) Dissanayake, A. L.; Jun, I.; Socolofsky, S. A. Numerical Models to Simulate Oil and Gas Blowout Plumes and Associated Chemical and Physical Processes of Hydrocarbons. In *E-Proceedings of the 36th IAHR World Congress*; The Hague, 2015.
(46) Gros, J.; Socolofsky, S. A.; Dissanayake, A. L.; Jun, I.; Zhao, L.; Boufadel, M. C.; Reddy, C. M.; Arey, J. S. Petroleum Dynamics in the Sea and Influence of Subsea Dispersant Injection during *Deepwater Horizon*. *Proc. Natl. Acad. Sci. U. S. A.* **2017**, *114*, 10065.
(47) Gros, J.; Reddy, C. M.; Nelson, R. K.; Socolofsky, S. A.; Arey, J. S. Simulating Gas−Liquid−Water Partitioning and Fluid Properties of Petroleum under Pressure: Implications for Deep-Sea Blowouts. *Environ. Sci. Technol.* **2016**, *50* (14), 7397−7408.
(48) Socolofsky, S. A.; Dissanayake, A. L.; Jun, I.; Gros, J.; Arey, J. S.; Reddy, C. M. Texas A&M Oilspill Calculator (TAMOC) Modeling Suite for Subsea Spills. In *Proceedings of the Thirty-Eighth AMOP Technical Seminar*; Environment Canada: Ottawa, 2015; pp 153−168.

DOI: 10.1021/acs.est.9b02131
Environ. Sci. Technol. 2019, 53, 10258−10268

(49) Socolofsky, S. A. *TAMOC*; Texas A&M University: College Station, 2017.
(50) Jun, I. A Numerical Model for Hydrocarbon Bubbles from Natural Seeps within Hydrate Stability Zone. Ph.D. Dissertation, Texas A&M University: College Station, TX, 2018.
(51) Zeebe, R.; Wolf-Gladrow, D. *CO_2 in Seawater: Equilibrium, Kinetics, Isotopes*; Elsevier Science, 2001; p 346.
(52) Esposito, A.; Giordano, G.; Anzidei, M. The 2002−2003 Submarine Gas Eruption at Panarea Volcano (Aeolian Islands, Italy): Volcanology of the Seafloor and Implications for the Hazard Scenario. *Mar. Geol.* **2006**, *227* (1), 119−134.
(53) Dekov, V. M.; Savelli, C. Hydrothermal Activity in the SE Tyrrhenian Sea: An Overview of 30 Years of Research. *Mar. Geol.* **2004**, *204* (1), 161−185.
(54) Mücke, I. Analysis of CO_2 Bubble Plumes East of Panarea: New Insights on Bubble Plume Dynamics and Seep Distribution. Master's Thesis, Christian-Albrechts-Universität zu Kiel: Kiel, 2017.
(55) McGinnis, D. F.; Beaubien, S. E.; Bigalke, N.; Bryant, L. D.; Celussi, M.; Comici, C.; De Vittor, C.; Feldens, P.; Giani, M.; Karuza, A.; et al. *The Panarea Natural CO_2 Seeps: Fate and Impact of the Leaking Gas ($PaCO_2$)*; Eurofleet's Cruise Report U10/2011; IFM-GEOMAR: Kiel, Germany, 2011; p 55.
(56) Caliro, S.; Caracausi, A.; Chiodini, G.; Ditta, M.; Italiano, F.; Longo, M.; Minopoli, C.; Nuccio, P. M.; Paonita, A.; Rizzo, A. Evidence of a Recent Input of Magmatic Gases into the Quiescent Volcanic Edifice of Panarea, Aeolian Islands, Italy. *Geophys. Res. Lett.* **2004**, *31* (7), 1.
(57) Capaccioni, B.; Tassi, F.; Vaselli, O.; Tedesco, D.; Poreda, R. Submarine Gas Burst at Panarea Island (Southern Italy) on 3 November 2002: A Magmatic versus Hydrothermal Episode. *J. Geophys. Res.* **2007**, *112* (B5), 1 DOI: 10.1029/2006JB004359.
(58) Clift, R.; Grace, J. R.; Weber, M. E. *Bubbles, Drops, and Particles*; Academic Press: New York, 1978.
(59) Leifer, I.; Patro, R. K. The Bubble Mechanism for Methane Transport from the Shallow Sea Bed to the Surface: A Review and Sensitivity Study. *Cont. Shelf Res.* **2002**, *22* (16), 2409−2428.
(60) Sam, A.; Gomez, C. O.; Finch, J. A. Axial Velocity Profiles of Single Bubbles in Water/Frother Solutions. *Int. J. Miner. Process.* **1996**, *47* (3), 177−196.
(61) Jordt, A.; Zelenka, C.; von Deimling, J. S.; Koch, R.; Köser, K. The Bubble Box: Towards an Automated Visual Sensor for 3D Analysis and Characterization of Marine Gas Release Sites. *Sensors* **2015**, *15* (12), 30716−30735.
(62) Wang, B.; Socolofsky, S. A. A Deep-Sea, High-Speed, Stereoscopic Imaging System for in Situ Measurement of Natural Seep Bubble and Droplet Characteristics. *Deep Sea Res., Part I* **2015**, *104*, 134−148.
(63) Abegg, F.; Linke, P. Remotely Operated Vehicle "ROV PHOCA". *J. Large-Scale Res. Facil. JLSRF* **2017**, *3* (0), 118.
(64) Leonte, M.; Wang, B.; Socolofsky, S. A.; Mau, S.; Breier, J. A.; Kessler, J. D. Using Carbon Isotope Fractionation to Constrain the Extent of Methane Dissolution into the Water Column Surrounding a Natural Hydrocarbon Gas Seep in the Northern Gulf of Mexico. *Geochem., Geophys., Geosyst.* **2018**, *19* (11), 4459−4475.
(65) *The Use of Dispersants in Marine Oil Spill Response*, National Academies Press: Washington, DC, 2019. DOI: 10.17226/25161.
(66) Peng, D.-Y.; Robinson, D. B. A New Two-Constant Equation of State. *Ind. Eng. Chem. Fundam.* **1976**, *15* (1), 59−64.
(67) Robinson, D. B.; Peng, D.-Y. *The Characterization of the Heptanes and Heavier Fractions for the GPA Peng-Robinson Programs*; Research Report 28; Gas Processors Association: Tulsa, 1978.
(68) Lin, H.; Duan, Y.-Y. Empirical Correction to the Peng−Robinson Equation of State for the Saturated Region. *Fluid Phase Equilib.* **2005**, *233* (2), 194−203.
(69) King, M. B. *Phase Equilibrium in Mixtures*; Danckwerts, P. V., Ed.; International series of monographs in chemical engineering; Pergamon press: Oxford, 1969.
(70) Dhima, A.; de Hemptinne, J.-C.; Jose, J. Solubility of Hydrocarbons and CO_2 Mixtures in Water under High Pressure. *Ind. Eng. Chem. Res.* **1999**, *38* (8), 3144−3161.
(71) Schwarzenbach, R. P.; Gschwend, P. M.; Imboden, D. M. *Environmental Organic Chemistry*, 2nd ed.; John Wiley & Sons, Inc.: Hoboken, 2003.
(72) Sander, R. Compilation of Henry's Law Constants, Version 3.99. *Atmos. Chem. Phys. Discuss.* **2014**, *14* (21), 29615−30521.
(73) Brown, P. N.; Byrne, G. D.; Hindmarsh, A. C. VODE: A Variable-Coefficient ODE Solver. *SIAM J. Sci. Stat Comput* **1989**, *10* (5), 1038−1051.
(74) McGinnis, D. F.; Greinert, J.; Artemov, Y.; Beaubien, S. E.; Wüest, A. Fate of Rising Methane Bubbles in Stratified Waters: How Much Methane Reaches the Atmosphere? *J. Geophys. Res.* **2006**, *111* (C9), C09007.
(75) Johnson, A. I.; Besik, F.; Hamielec, A. E. Mass Transfer from a Single Rising Bubble. *Can. J. Chem. Eng.* **1969**, *47*, 559−564.
(76) Rehder, G.; Brewer, P. W.; Peltzer, E. T.; Friederich, G. Enhanced Lifetime of Methane Bubble Streams within the Deep Ocean. *Geophys. Res. Lett.* **2002**, *29* (15), 21-1−21-24.
(77) McGinnis, D. F.; Little, J. C. Predicting Diffused-Bubble Oxygen Transfer Rate Using the Discrete-Bubble Model. *Water Res.* **2002**, *36* (18), 4627−4635.
(78) Rehder, G.; Leifer, I.; Brewer, P. G.; Friederich, G.; Peltzer, E. T. Controls on Methane Bubble Dissolution inside and Outside the Hydrate Stability Field from Open Ocean Field Experiments and Numerical Modeling. *Mar. Chem.* **2009**, *114* (1−2), 19−30.
(79) Zheng, L.; Yapa, P. D. Modeling Gas Dissolution in Deepwater Oil/Gas Spills. *J. Mar. Syst.* **2002**, *31* (4), 299−309.
(80) Hamme, R. C.; Emerson, S. R. The Solubility of Neon, Nitrogen and Argon in Distilled Water and Seawater. *Deep Sea Res., Part I* **2004**, *51* (11), 1517−1528.
(81) Pilson, M. E. Q. *An Introduction to the Chemistry of the Sea*, 2nd ed.; Cambridge University Press: Cambridge, 2013.
(82) Greenwood, J.; Craig, P.; Hardman-Mountford, N. Coastal Monitoring Strategy for Geochemical Detection of Fugitive CO_2 Seeps from the Seabed. *Int. J. Greenhouse Gas Control* **2015**, *39*, 74−78.
(83) French McCay, D.; Jayko, K.; Li, Z.; Horn, M.; Kim, Y.; Isaji, T.; Crowley, D.; Spaulding, M.; Decker, L.; Turner, C.; et al. *Technical Reports for Deepwater Horizon Water Column Injury Assessment WC_TR.14: Modeling Oil Fate and Exposure Concentrations in the Deepwater Plume and Rising Oil Resulting from the Deepwater Horizon Oil Spill*; RPS ASA: South Kingstown, 2015; p 536.
(84) van Sebille, E.; Griffies, S. M.; Abernathey, R.; Adams, T. P.; Berloff, P.; Biastoch, A.; Blanke, B.; Chassignet, E. P.; Cheng, Y.; Cotter, C. J.; et al. Lagrangian Ocean Analysis: Fundamentals and Practices. *Ocean Model.* **2018**, *121*, 49−75.
(85) Socolofsky, S. A.; Jirka, G. H. *Special Topics in Mixing and Transport Processes in the Environment*, 5th ed.; Texas A&M University: College Station, TX, 2005.
(86) Fischer, H. B.; List, E. J.; Koh, R. C. Y.; Imberger, J.; Brooks, N. H. *Mixing in Inland and Coastal Waters*; Academic Press: London, 1979.
(87) Okubo, A. *Some Speculations on Oceanic Diffusion Diagrams*; Symposium on The Physical Processes Responsible for the Dispersal of Pollutants in the Sea with Special Reference to the Nearshore Zone, 1972.
(88) Blackford, J.; Stahl, H.; Bull, J. M.; Bergès, B. J. P.; Cevatoglu, M.; Lichtschlag, A.; Connelly, D.; James, R. H.; Kita, J.; Long, D.; et al. Detection and Impacts of Leakage from Sub-Seafloor Deep Geological Carbon Dioxide Storage. *Nat. Clim. Change* **2014**, *4* (11), 1011−1016.
(89) Molari, M.; Guilini, K.; Lott, C.; Weber, M.; de Beer, D.; Meyer, S.; Ramette, A.; Wegener, G.; Wenzhöfer, F.; Martin, D.; et al. CO_2 Leakage Alters Biogeochemical and Ecological Functions of Submarine Sands. *Sci. Adv.* **2018**, *4* (2), eaao2040.

DOI: 10.1021/acs.est.9b02131
Environ. Sci. Technol. 2019, 53, 10258−10268

(90) Schneider, A.; Wallace, D. W. R.; Körtzinger, A. Alkalinity of the Mediterranean Sea. *Geophys. Res. Lett.* **2007**, *34* (15), 1 DOI: 10.1029/2006GL028842.
(91) Orr, J. C.; Epitalon, J.-M.; Gattuso, J.-P. Comparison of Ten Packages That Compute Ocean Carbonate Chemistry. *Biogeosciences* **2015**, *12* (5), 1483−1510.
(92) Carpenter, J.; Bithell, J. Bootstrap Confidence Intervals: When, Which, What? A Practical Guide for Medical Statisticians. *Stat. Med.* **2000**, *19* (9), 1141−1164.
(93) Johansen, C.; Todd, A. C.; MacDonald, I. R. Time Series Video Analysis of Bubble Release Processes at Natural Hydrocarbon Seeps in the Northern Gulf of Mexico. *Mar. Pet. Geol.* **2017**, *82*, 21−34.
(94) Römer, M.; Sahling, H.; Pape, T.; Bohrmann, G.; Spieß, V. Quantification of Gas Bubble Emissions from Submarine Hydrocarbon Seeps at the Makran Continental Margin (Offshore Pakistan). *J. Geophys. Res. Oceans* **2012**, *117* (C10), 1.
(95) Riedel, M.; Scherwath, M.; Römer, M.; Veloso, M.; Heesemann, M.; Spence, G. D. Distributed Natural Gas Venting Offshore along the Cascadia Margin. *Nat. Commun.* **2018**, *9* (1), 3264.
(96) Leifer, I. Characteristics and Scaling of Bubble Plumes from Marine Hydrocarbon Seepage in the Coal Oil Point Seep Field. *J. Geophys. Res.* **2010**, *115* (C11), 1−20.
(97) Leifer, I.; Patro, R. K.; Bowyer, P. A Study on the Temperature Variation of Rise Velocity for Large Clean Bubbles. *J. Atmospheric Ocean. Technol.* **2000**, *17* (10), 1392−1402.
(98) DelSontro, T.; McGinnis, D. F.; Wehrli, B.; Ostrovsky, I. Size Does Matter: Importance of Large Bubbles and Small-Scale Hot Spots for Methane Transport. *Environ. Sci. Technol.* **2015**, *49* (3), 1268−1276.
(99) Brewer, P. G.; Peltzer, E. T.; Friederich, G.; Rehder, G. Experimental Determination of the Fate of Rising CO_2 Droplets in Seawater. *Environ. Sci. Technol.* **2002**, *36* (24), 5441−5446.
(100) Socolofsky, S. A.; Bhaumik, T. Dissolution of Direct Ocean Carbon Sequestration Plumes Using an Integral Model Approach. *J. Hydraul. Eng.* **2008**, *134* (11), 1570−1578.
(101) *Environmental Trends in Germany, Data on the Environment 2015*; Federal Environment Agency of Germany, Section I 1.5: Dessau-Roßlau, 2015; p 142.
(102) Wang, B.; Socolofsky, S. A.; Lai, C. C. K.; Adams, E. E.; Boufadel, M. C. Behavior and Dynamics of Bubble Breakup in Gas Pipeline Leaks and Accidental Subsea Oil Well Blowouts. *Mar. Pollut. Bull.* **2018**, *131*, 72−86.
(103) Zhao, L.; Boufadel, M. C.; Socolofsky, S. A.; Adams, E.; King, T.; Lee, K. Evolution of Droplets in Subsea Oil and Gas Blowouts: Development and Validation of the Numerical Model VDROP. *Mar. Pollut. Bull.* **2014**, *83* (1), 58−69.
(104) Zhao, L.; Boufadel, M. C.; King, T.; Robinson, B.; Gao, F.; Socolofsky, S. A.; Lee, K. Droplet and Bubble Formation of Combined Oil and Gas Releases in Subsea Blowouts. *Mar. Pollut. Bull.* **2017**, *120* (1), 203−216.
(105) Widdicombe, S.; Blackford, J. C.; Spicer, J. I. Assessing the Environmental Consequences of CO_2 Leakage from Geological CCS: Generating Evidence to Support Environmental Risk Assessment. *Mar. Pollut. Bull.* **2013**, *73* (2), 399−401.
(106) Guilini, K.; Weber, M.; de Beer, D.; Schneider, M.; Molari, M.; Lott, C.; Bodnar, W.; Mascart, T.; Troch, M. D.; Vanreusel, A. Response of *Posidonia Oceanica* Seagrass and Its Epibiont Communities to Ocean Acidification. *PLoS One* **2017**, *12* (8), e0181531.
(107) Tyrrell, T. Calcium Carbonate Cycling in Future Oceans and Its Influence on Future Climates. *J. Plankton Res.* **2008**, *30* (2), 141−156.
(108) Millero, F. J. The Marine Inorganic Carbon Cycle. *Chem. Rev.* **2007**, *107* (2), 308−341.
(109) Kroeker, K. J.; Kordas, R. L.; Crim, R.; Hendriks, I. E.; Ramajo, L.; Singh, G. S.; Duarte, C. M.; Gattuso, J.-P. Impacts of Ocean Acidification on Marine Organisms: Quantifying Sensitivities and Interaction with Warming. *Glob. Change Biol.* **2013**, *19* (6), 1884−1896.
(110) Pandolfi, J. M.; Connolly, S. R.; Marshall, D. J.; Cohen, A. L. Projecting Coral Reef Futures Under Global Warming and Ocean Acidification. *Science* **2011**, *333* (6041), 418−422.
(111) Guinotte, J. M.; Fabry, V. J. Ocean Acidification and Its Potential Effects on Marine Ecosystems. *Ann. N. Y. Acad. Sci.* **2008**, *1134* (1), 320−342.
(112) Anzidei, M.; Esposito, A.; Bortoluzzi, G.; De Giosa, F. The High Resolution Bathymetric Map of the Exhalative Area of Panarea (Aeolian Islands, Italy). *Ann. Geophys.* **2005**, *48* (6), 1 DOI: 10.4401/ag-3242.

DOI: 10.1021/acs.est.9b02131
Environ. Sci. Technol. 2019, 53, 10258−10268